Eur. J. Biochem. **266**, 444–452 (1999) © FEBS 1999

Supramolecular organization of photosystem II and its light-harvesting antenna in partially solubilized photosystem II membranes

Egbert J. Boekema[1], Henny van Roon[2], Jan F. L. van Breemen[1] and Jan P. Dekker[2]

[1]*Department of Biophysical Chemistry, Groningen Biomolecular Sciences and Biotechnology Institute, University of Groningen, the Netherlands;* [2]*Division of Physics and Astronomy, Institute of Molecular Biological Sciences, Vrije Universiteit, Amsterdam, the Netherlands*

We present an extended analysis of the organization of green plant photosystem II and its associated light-harvesting antenna using electron microscopy and image analysis. The analysis is based on a large dataset of 16 600 projections of negatively stained PSII–LHCII supercomplexes and megacomplexes prepared by means of three different pretreatments. In addition to our previous work on this system [Boekema, E.J., van Roon, H., Calkoen, F., Bassi, R. and Dekker, J.P. (1999) *Biochemistry* **38**, 2233–2239], the following results were obtained.

The rotational orientation of trimeric LHCII at the S, M and L binding positions was determined. It was found that compared to the S trimer, the M and L trimers are rotationally shifted by about −20° and −50°, respectively.

The number of projections with empty CP29, CP26 and CP24 binding sites was found to be about 0, 18 and 4%, respectively. We suggest that CP26 and CP24 are not required for the binding of trimeric LHCII at any of the three binding positions.

A new type of megacomplex was observed with a characteristic windmill-like shape. This type III megacomplex consists of two C_2S_2 supercomplexes connected at their CP26 tips.

Structural variation in the region of the central dimeric photosystem II complex was found to occur at one specific position near the periphery of the complex. We attribute this variation to the partial absence of an extrinsic polypeptide or one or more small intrinsic membrane proteins.

Keywords: photosystem II; light harvesting complex; thylakoid membrane; electron microscopy.

A key role in the energy-conserving mechanisms of green plants is played by photosystem II (PSII). Its major task is to use light energy for the reduction of plastoquinone, the oxidation of water and the formation of a transmembrane pH gradient. It consists of at least 25 different types of protein subunits [1], which are organized into two structurally and functionally distinct parts. The first part is the core complex, a well-defined structure that is responsible for all electron transfer reactions in PSII, including the formation of oxygen. It contains the reaction centre proteins D1 and D2, cytochrome *b*-559, two core antenna proteins called CP47 and CP43, a number of extrinsic proteins indirectly involved in the oxygen-evolving process, and several small proteins of unknown function [1]. There is overwhelming evidence that the PSII core complex is organized as a dimer in the stacked, appressed regions of the thylakoid membrane [2–4]. The structure of the PSII core complex without the CP43 subunit has been determined at 8 Å resolution by electron crystallography on two-dimensional crystals [5,6]. The structure reveals 23 transmembrane α-helices [7], of which six have been assigned to CP47, and 10 to the D1 and D2 proteins. Two of the remaining seven transmembrane α-helices are probably formed by cytochrome *b*-559, while the others are thought to belong to small proteins consisting of a single transmembrane α-helix [6].

The second part of PSII is the peripheral antenna, which in green plants and algae consists of an unknown structure of several light-harvesting complex II (LHCII) proteins and which absorbs most of the sunlight to be directed to the photochemical reaction centre of PSII [8]. The LHCII proteins are encoded by the related nuclear genes designated *Lhcb1–6*. *Lhcb1* forms trimeric complexes with *Lhcb2* or *Lhcb3*, while the three other proteins *Lhcb4* (CP29), *Lhcb5* (CP26) and *Lhcb6* (CP24) are monomeric [8,9]. The structure of the trimeric LHCII complex is known at 3.4 Å resolution [10,11], revealing the positions of three trans-membrane α-helices, 12 chlorophylls and two xanthophylls, and it is thought that the monomeric LHCII proteins give rise to very similar structures [12]. The LHCII proteins play a key role in the formation of the stacked grana membranes in the thylakoids and they are also heavily involved in a number of regulatory processes [8], such as the regulation of the energy distribution between the two photosystems via (de)phosphorylation reactions of *Lhcb1* and *Lhcb2* and the harmless dissipation of excess excitation energy into heat under conditions of light stress.

The first details of the organization of trimeric and monomeric LHCII around the PSII core complex were provided by the characterization of a PSII–LHCII supercomplex by electron microscopy and image analysis [13]. The data indicated a dimeric PSII core complex surrounded by two peripheral antenna structures in symmetry-related positions,

Correspondence to J. P. Dekker, Faculty of Sciences, Division of Physics and Astronomy, Vrije Universiteit, De Boelelaan 1081, 1081 HV Amsterdam, the Netherlands. Fax: + 31 20 4447999, Tel.: + 31 20 4447931, E-mail: dekker@nat.vu.nl

Abbreviations: α-DM, *n*-dodecyl-α,D-maltoside; β-DM, *n*-dodecyl-β,D-maltoside; C, PSII core complex; LHCII, light harvesting complex II; L, loosely bound trimeric LHCII; M, moderately bound trimeric LHCII; OEC, oxygen-evolving complex; PSII, photosystem II; RC, reaction centre; S, strongly bound trimeric LHCII.

(Received 12 July 1999, revised 17 September 1999, accepted 20 September 1999)

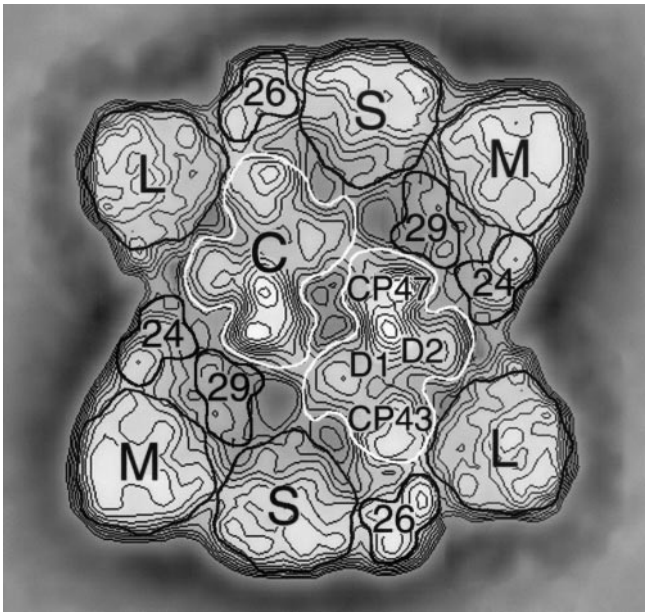

Fig. 1. Organization of the hypothetical $C_2S_2M_2L_2$ supercomplex. Constructed image of a 'complete' PSII–LHCII supercomplex. The boundaries of the PSII core complex are depicted in white, whereas those of the various antenna complexes are depicted in black. C, PSII core complex; S, strongly bound LHCII; M, moderately bound LHCII; L, loosely bound LHCII; 29, CP29; 26, CP26; 24, CP24. The right-hand PSII core complex shows the locations of its four largest subunits.

each consisting of one trimeric and two monomeric LHCII complexes. Biochemical analysis identified the monomeric LHCII proteins as CP29 and CP26 and the trimeric LHCII as a complex of the *Lhcb1* and *Lhcb2* gene products [14]. This complex has recently been purified at high yield directly from thylakoid membranes [15], and may be regarded as a basic building block of PSII *in vivo*. Cross-linking studies on an even larger supercomplex suggested the specific locations of the CP29 and CP26 proteins; locations for CP24 and a second trimeric LHCII complex were also proposed [16]. Studies on PSII–LHCII supercomplexes have also increased our knowledge on the positions of the extrinsic proteins involved in oxygen evolution [13,17].

Recently, we started to investigate the supramolecular organization of the PSII core and its associated peripheral antenna by electron microscopy and image analysis on partially solubilized PSII grana membranes [18–20]. We used the very mild detergent *n*-dodecyl-α,D-maltoside (α-DM) for this purpose, and reduced the amount of detergent and the time of detergent exposure to an absolute minimum to prevent the fragmentation of the fragile supramolecular complexes as much as possible. The studies revealed the presence of supercomplexes consisting of a dimeric PSII core complex (designated 'C_2' in our terminology) and trimeric LHCII in three different types of binding positions ('S', 'M' and 'L', referring to strongly, moderately and loosely bound LHCII, respectively). In addition, two types of 'megacomplexes' were found, which were both identified as associations of two C_2S_2M supercomplexes [19], as well as a heptameric association of trimeric LHCII, the so-called icosienamer [20]. Figure 1 summarizes the most important findings of this earlier work and shows the binding positions of the S, M, and L trimers, as well as those of the monomeric CP29, CP26 and CP24 proteins. We note that this 'complete' PSII–LHCII supercomplex with six trimeric LHCII units around a dimeric PSII core has not yet been observed. Supercomplexes with five trimeric LHCII units have been observed, but in very small amounts [19].

In this report we present new details of the analysis of α-DM-solubilized PSII membranes. A very large data set of 16 600 projections was investigated, which allowed the determination of structural details like the rotational orientation of trimeric LHCII in the three binding positions, the variance of the occupancy of the sites attributed to the monomeric LHC proteins CP29, CP26 and CP24 and the structural variation in the PSII core parts. Part of the work described in this paper has been presented at the XIth International Congress on Photosynthesis in Budapest, 1998 [21,22].

MATERIALS AND METHODS

Oxygen-evolving PSII membranes were isolated from freshly prepared thylakoid membranes from spinach as described previously [23] with modifications as described in [19]. In short, the membranes (at a final chlorophyll concentration of 1.9 mg mL^{-1}) were partially solubilized with *n*-dodecyl-α, D-maltoside (α-DM, final concentration 1.2%), centrifuged to remove unsolubilized material, partially purified by gel-filtration chromatography using a Superdex 200 HR 10/30 column (Pharmacia) as described in [19] or by sucrose density gradient centrifugation (see below), and immediately prepared for electron microscopy as described in [19]. For the separation by sucrose density gradient centrifugation, the solubilized fraction was layered on a 8–45% sucrose gradient in bisTris/taurine/α-DM buffer (20 mM bisTris, 20 mM NaCl, 10 mM $MgCl_2$, 1.5% taurine and 0.03% α-DM) at pH 6.5. The gradient was run for 16 h in a Beckman SW41 rotor at 200 000 ***g*** (4 °C). A pronounced green band was harvested from the 30% layer and analysed by diode-array-assisted gel-filtration chromatography as described in [24]. This band was found to consist of a collection of supercomplexes characterized by A_{470}/A_{435} ratios ranging from 0.46 to 0.58 [18]. The harvested material was largely devoid of megacomplexes, trimeric, monomeric LHCII particles. The supercomplexes were desalted on a PD10 column equilibrated in bisTris/α-DM buffer (buffer as above lacking taurine) and immediately prepared for electron microscopy as in [18].

Transmission electron microscopy was performed with a Philips CM10 electron microscope at 52 000× magnification. Negatively stained specimens were prepared on glow-discharged carbon-coated copper grids as described in [19]. Micrographs were digitized with a Kodak Eikonix Model 1412 CCD camera with a step size of 25 μm, corresponding to a pixel size of 0.485 nm at the specimen level. Projections were extracted for image analysis with IMAGIC software [25] following alignment procedures and treatment by multivariate statistical analysis and classification as described previously [13,19,25]. The resolution of the images was estimated by using the Fourier ring correlation method [26] and was found to be 16.5 Å for the most abundant projections [18,19].

RESULTS AND DISCUSSION

Image analysis

In order to investigate the supramolecular organization of PSII and its associated light-harvesting antenna, a total number of 16 600 single particle top-view projections of PSII–LHCII supercomplexes and megacomplexes were extracted from negatively stained electron microscopy images. The dataset,

Table 1. Relative occurrence of the various PSII–LHCII supercomplexes and megacomplexes. The numbers are based on four datasets (see text) of 16 600 projections, of which 12 410 could be assigned to any of the groups mentioned in this table. The number of 12 755 assigned projections is based on an extrapolation of the number of C_2SM particles in the complete dataset.

Complex	No. assigned projections	% Projections
Total	12 755	100
C_2S_2	9000	70.6
C_2SM	920[a]	7.2
C_2S_2M	1860	14.6
$C_2S_2M_2$	120	0.9
C_2S_2L	85	0.7
$C_2S_2L_2$	6	0.05
C_2S_2ML	85	0.7
Mega I ($C_4S_4M_{2-4}$)	360	2.8
Mega II ($C_4S_4M_{2-4}$)	170	1.3
Mega III (C_4S_4)	39	0.3
Icosienamer (X_7)	110	0.9
Total S	25 508	100
Total M	4202	16.5
Total L	182	0.7
Total CP29		100[b]
Total CP26		81.9[c]
Total CP24		16.5[d]/96.2[e]

[a] Number based on an extrapolation of its occurrence in the first and second datasets to the complete set. [b] Assumed to be equal to 'Total S'. [c] Calculated from the first dataset and the datasets of the type I megacomplexes, as for these sets all CP26-free projections have certainly been selected. [d] Percentage based on 'Total S'. [e] Percentage based on 'Total M' + 'Total L'.

on which the work described in this paper is based, is a combination of four sets, obtained from supercomplexes and megacomplexes prepared in three slightly different ways. The first set of 2950 projections was obtained from particles prepared for electron microscopy without any purification as described in [18]. The second set consisted of 4500 projections and was obtained from particles that were partially purified by means of sucrose density gradient centrifugation (see Materials and methods), while the third and fourth sets (7300 and 1850 projections, respectively) originated from particles that were partially purified by gel-filtration chromatography as described in [19]. The first and third datasets formed the basis of the work presented in [18,19], respectively.

The purpose of this paper is to present an extended overview and re-analysis of the features of the various types of supercomplexes and megacomplexes in the current datasets. The numbers of selected types of supercomplexes and megacomplexes are presented in Table 1. The majority of all selected particles consists of the 'standard' PSII–LHCII supercomplexes [13], called C_2S_2 in our nomenclature [18]. As even the fastest computers are not yet able to compare 16 600 projections simultaneously by multivariate statistical analysis, we decided, after collecting the first half of the data, not to further select all particles lacking mass at the left-upper and/or right-lower tips (the CP26 protein, see below). Furthermore, we note that the smaller C_2S particle is not considered in this work (although it was included in the initial dataset in [18]), and that the C_2SM supercomplex was only extracted from the first and second datasets. Otherwise, the numbers of particles, presented in Table 1, give a fairly good impression about the relative abundance of supercomplexes and megacomplexes, of which various features will be described and discussed below.

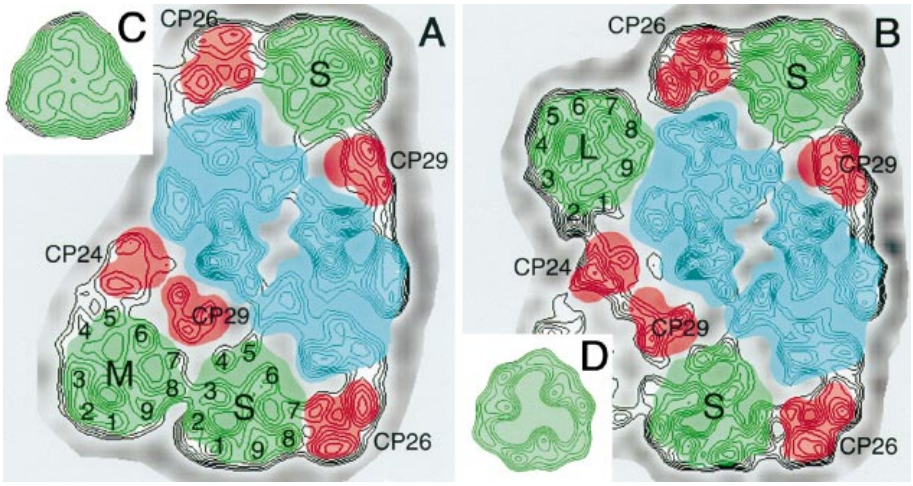

Fig. 2. Rotational orientation of trimeric LHCII in the S, M and L binding positions. High-pass filtered images to suppress the effect of the stain gradient on the structure details below 30 Å. (A) High-pass filtered image of C_2S_2M, obtained after summation of the isolated C_2S_2M supercomplexes and the C_2S_2M parts of the type I and type II megacomplexes [19]. The PSII core, monomeric LHCII and trimeric LHCII parts are indicated in blue, red and green, respectively. Nine densities are visible in the trimeric LHCII regions, which were numbered 1–9 as previously [20]. (B) High-pass filtered image of C_2S_2L, obtained after summation of the isolated C_2S_2L and C_2S_2ML supercomplexes [19]. (C) Image of the S-LHCII trimer, obtained by threefold symmetrization of the lower S trimer shown in (A). The green overlayer indicates the fit of this trimer with the trimer presented in (D). (D) The unstained projection map of the LHCII trimer from pea, positioned in such a way that the overlap with the S trimer in (C) is maximal. The image was obtained using data from [27], the original image was generated by truncating the 0.7 nm projection map at 1.6 nm resolution.

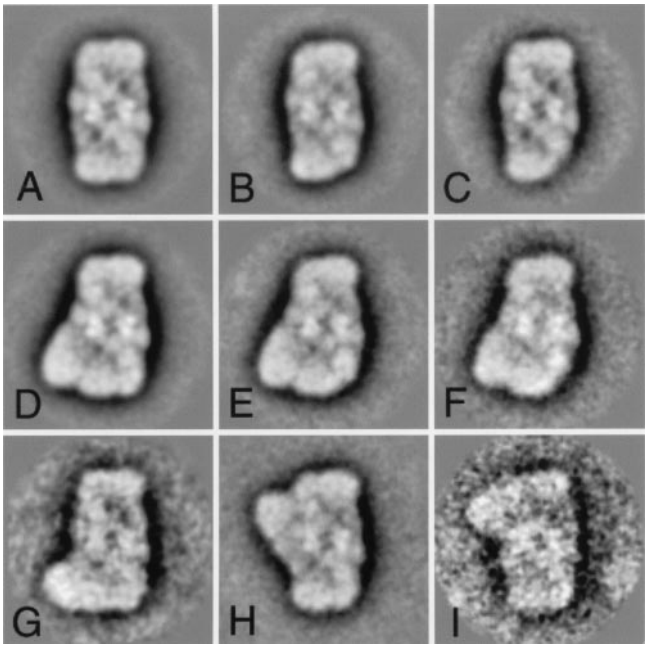

Fig. 3. Average projections of nine characteristics types of PSII–LHCII supercomplexes. (A) Average of the best 600 dimeric C_2S_2 supercomplexes. (B) Average of 183 C_2S_2 supercomplexes lacking a small mass at the lower right CP26 tip. (C) Average of 120 C_2S_2 supercomplexes lacking a large mass at the lower right tip. (D) Average of the best 360 C_2S_2M supercomplexes. (E) Average of 111 C_2S_2M supercomplexes lacking a small mass at the lower right tip. (F) Average of 43 C_2S_2M supercomplexes lacking a large mass at the lower right tip. (G) Average of 21 C_2S_2M supercomplexes lacking mass of the size of a monomeric protein at the middle left. (H) Average of 85 C_2S_2L supercomplexes. (I) Average of 9 C_2S_2L supercomplexes lacking mass of the size of a monomeric protein at the middle left. No rotational symmetry was imposed on the images.

Rotational positioning of trimeric LHCII

In our previous report, we showed that structural detail had become visible at 16.5 Å in the best averaged projections of the PSII–LHCII supercomplexes and that several new densities had been revealed [19], which could, for instance, give new information on the rotational positioning of the trimeric antenna proteins. However, a comparison of the various complexes learns that less detail can be observed in the trimeric LHCII parts of the PSII–LHCII supercomplexes than of the icosienamers (cf. Fig. 1 and [20]). The latter particles clearly show a stain-excluding tripod in the middle and three stain-excluding masses between the legs of the tripod in the periphery. Very similar features were observed in negatively stained two-dimensional LHCII crystals [27]. We attribute the lower visibility of trimeric LHCII in the PSII–LHCII supercomplexes to a more uneven distribution of negative stain in PSII–LHCII supercomplexes than in LHCII-only structures, which can be caused by the nearby protrusions of the extrinsic proteins and the core antenna proteins in the PSII core parts of the supercomplexes.

In order to minimize the effect of the stain gradient and to enhance density positions, we applied a high-pass filter on the C_2S_2M unit (the sum of the isolated C_2S_2M particles and the C_2S_2M parts of the type I and type II megacomplexes; Fig. 2A) and the C_2S_2 L unit (the sum of the C_2S_2ML and C_2S_2 L particles; Fig. 2B). In the tentative positions of LHCII trimers of type S (Fig. 2A,B), type M (Fig. 2A) and type L (Fig. 2B), a nine-density profile is now revealed in all cases, which is, however, most clear for the innermost, S-type LHCII. The same procedure also led to a nine-density profile in each LHCII of the icosienamer [20]. The rotational orientation is most easily observed through the three symmetrically organized stained regions in the LHCII trimers. In the icosienameras presented in [20], these stained regions are easily observed and in each trimeric LHCII unit two of the three densities are almost parallel to the base of the particle. Comparison with the structures in Fig. 2, shows that the rotational orientation of the L-LHCII is virtually the same as that of the central LHCII unit in the icosienamer, and that the S-LHCII is shifted slightly anticlockwise compared to the base of the supercomplex (5–10°) and that the M-LHCII is shifted considerably anticlockwise (≈ 25°). A computer calculation of the rotational positioning of the LHCII trimer in the three different binding sites revealed that in comparison to the S-LHCII in the lower left corner, the LHCII trimers in the M and L positions differ by about −20° and −50°, respectively, inline with the above-mentioned qualitative consideration.

We conclude that the L-LHCII makes small angles with the S-LHCII in the upper half of the complex and that the rotational orientation of M-LHCII differs considerably from that of the two other trimeric LHCII complexes We note that the M-LHCII may have a unique polypeptide composition. Two groups have reported a supramolecular complex consisting of the *Lhcb1*, *Lhcb3*, *Lhcb4* (CP29) and *Lhcb6* (CP24) gene products in a ratio of 2 : 1 : 1 : 1 [28,29]. Because the M-LHCII is the only trimeric LHCII with close contacts to CP29 and CP24 (Fig. 1), *Lhcb3* is absent in the standard C_2S_2 supercomplexes [14], and *Lhcb3* seems to be located closely to the PSII core complex [28], it seems reasonable to assume that the M-LHCII is the only LHCII that binds the minor *Lhcb3* gene product.

In an attempt to assign the nine density profiles of the S-, M- and L-LHCII trimers, a comparison was made with the LHCII map from the high-resolution crystallographic studies from Kühlbrandt [27], presented at a comparable resolution. Its outer shape (Fig. 2D) correlates well with the shape of the threefold averaged S-trimer (Fig. 2C), despite the fact that different specimen preparation techniques

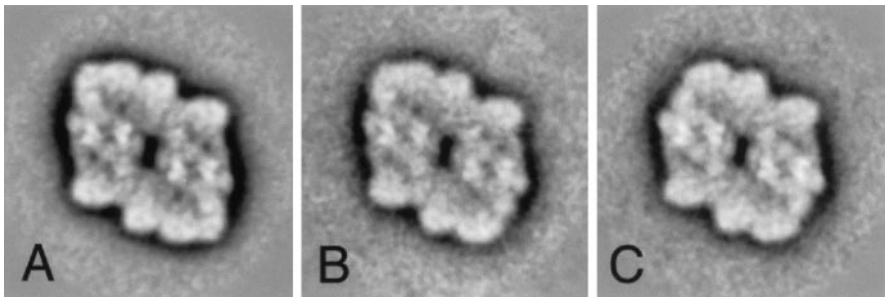

Fig. 4. Classification of 335 projections of type I C4S4M2 megacomplexes. (A) Sum of the best 130 projections (out of 147) from classes with complete CP26 tips at upper left and lower right corners. (B) Sum of 75 projections (out of 94) lacking the complete CP26 tip at the lower right position. (C) Sum of 42 projections (out of 70) lacking both CP26 tips.

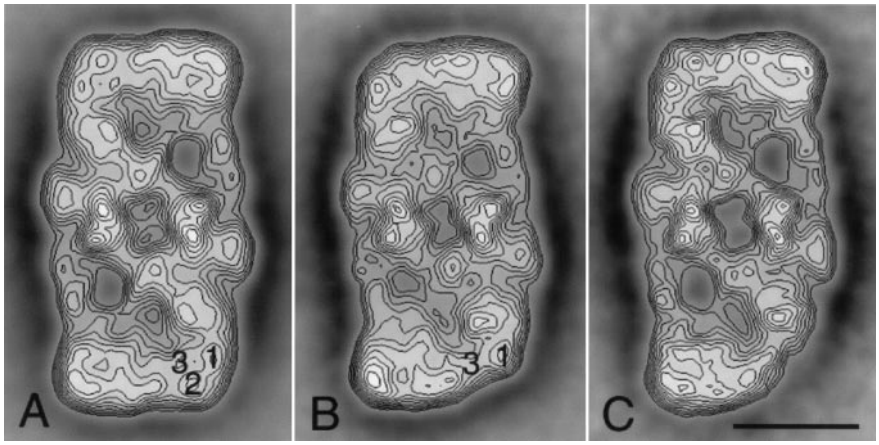

Fig. 5. Step-wise loss of the CP26 subunit from the C_2S_2 supercomplex. Contoured version of (A) the 'native/fresh' supercomplex (Fig. 3A) with the three CP26 domains indicated by numbers 1–3 (B) sucrose-gradient purified particles (Fig. 3B), lacking domain 2 in lowerright tip, and (C) particles lacking all three CP26 domains in the lower right part of the complex (Fig. 3C). Scale bar equals 10 nm.

(unstained/cryo versus negative stain) and averaging techniques (crystallographic versus a-periodic) were used. The positions of the strongest densities (3, 6 and 9) in the stain map (Fig. 2C) correlate well with the positions of the strongest densities in the high-resolution map. This would imply that most likely the densities 8-9-1, 2-3-4 and 5-6-7 coincide with the individual LHCII monomers. However, a comparison of stained and unstained crystal maps, as presented in [27], places the tripods of the stain map not in the expected 3-6-9 positions, but in a 1-4-7 position. This discrepancy, for which we have no explanation, makes an ultimate assignment uncertain at the present resolution and we will not therefore speculate further on the absolute rotational positions of the various trimeric LHCII complexes. It is of interest to note, however, that the shapes of the three types of LHCII trimers may deviate somewhat from exact threefold symmetry. Each type of LHCII shows one or two densities that fall partially outside the symmetric contour of the trimer (Fig. 1). The possible asymmetry can be caused by differences in interactions with the environment, or by heterogeneity in the subunit composition of the trimers.

Supercomplexes missing a monomeric LHCII protein

The most frequently occurring particles within each subset of projections have been shown and analysed in our previous report [19]. However, within all subsets specific variability was found, in particular in the regions where the monomeric LHCII proteins CP29, CP26 and CP24 are located. In this section, we describe the observed variability at these locations.

The lower right and upper left tips of the most frequently occurring structure (the standard C_2S_2 supercomplex; Fig. 3A) have been assigned to the CP26 protein [16], which appear as three density areas in the projected map of the C_2S_2 supercomplex (Fig. 5A) and other relatively well-defined supercomplexes. Classification of the large C_2S_2 subset, however, revealed that a minority of the projections belongs to two specific fragments in which either one (Figs 3B and 5B) or all densities at the CP26 position (Figs 3C and 5C) are absent. The fragments in Fig. 3B were observed predominantly in the sucrose density gradient prepurified material and were observed rarely in the nonpurified material [18]. Very similar features at the CP26 positions were observed after the classification of the C_2S_2M subset (Fig. 3D–F) and the subset of type I megacomplexes (Fig. 4A–C). The number of particles in the other subsets were too small to determine the variation at the CP26 position with accuracy. It is very likely, however, that the same types of variation occur in these subsets.

It is possible that the partial absence of mass at the CP26 tip (Fig. 3B) is caused by proteolysis. CP26 has been shown to be exceptionally vulnerable to proteolytic breakdown in isolated PSII–LHCII supercomplexes [15]. This possibility is in agreement with our observation that the partial absence of mass at the CP26 tip was observed predominantly after an overnight prepurification using a sucrose density gradient centrifugation and did not occur to a significant extent if the detergent exposure was limited to a few minutes [18]. We can only speculate on the importance of the occurrence of supercomplexes and megacomplexes with a completely empty

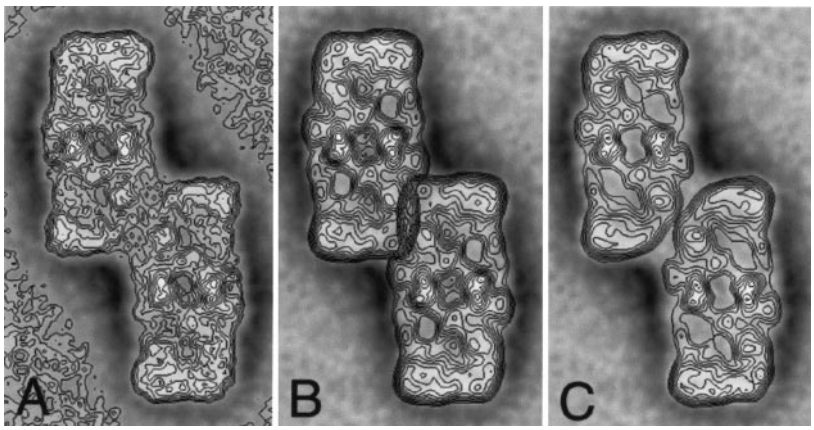

Fig. 6. Averaged projection of the type III megacomplex. This projection is the average of the best 39 projections of the type III (C_4S_4) megacomplex and is shown in (A) as a contoured version, in (B) with superimposed contour lines of two C_2S_2 supercomplexes (Fig. 5A) fitted into the positions of the two half-molecules and in (C) with superimposed contour lines of two C_2S_2 supercomplexes lacking the CP26 subunit (Fig. 5C).

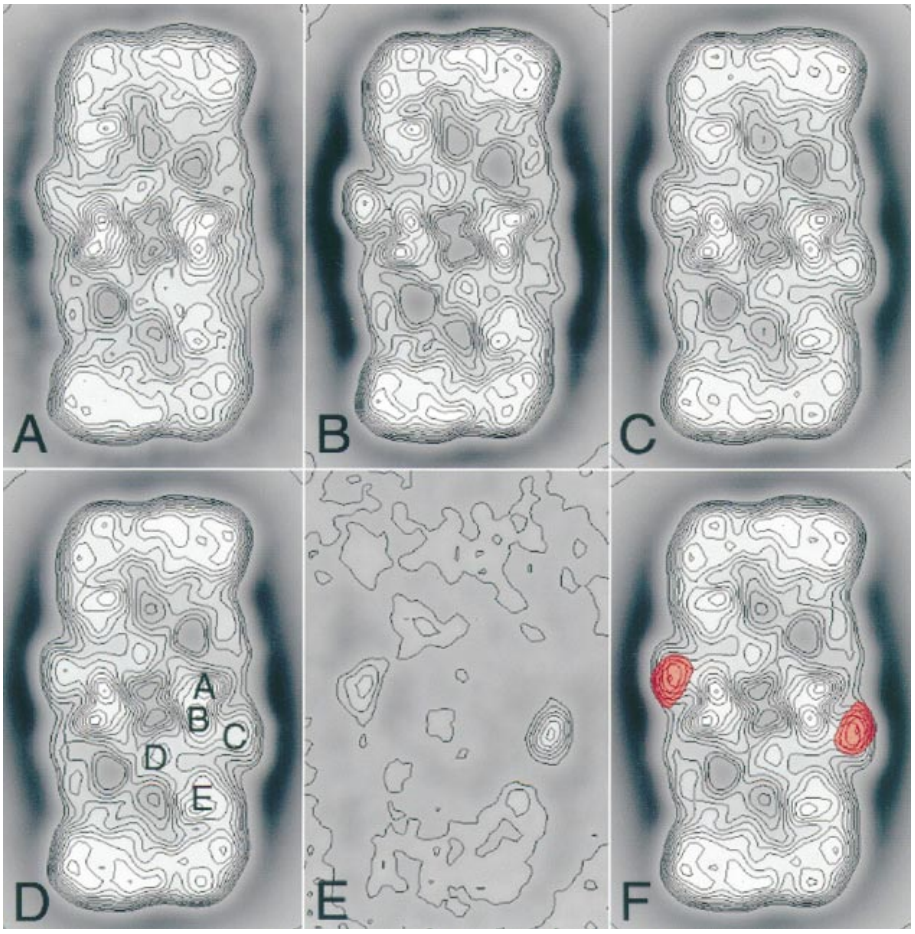

Fig. 7. Detection of a variably occupied density in the C_2S_2 supercomplex. Results were obtained from the classification of a set of 5600 C_2S_2 supercomplex projections from one isolation experiment (see also [19]). In an initial classification, about 25% of the projections with the lowest signal-to-noise ratio were removed, after which the remaining subset of 4273 better-preserved C_2S_2 supercomplexes was decomposed into 12 classes, which were checked for variation in the five densities A–E of the central core part (see D). (A) Sum of 327 projections of one class, strongly reduced in the two densities C. (B) Sum of 997 projections (three classes) with a reduced density C on the right side. (C) Sum of 2949 projections (the remaining eight classes) with twofold symmetry imposed. (D) Total sum of all projections (without symmetry); the letters A–E indicate the five densities as in [17]. A, CP47; B, 33 kDa protein; C, D2 (or D1); D, D1 (or D2); E, CP43. (E) Difference image between D and A. (F) The two high-difference areas of E (in red) imposed on the image of D, with twofold symmetry imposed.

CP26 site. The proteolysis may be less likely here because the number of complexes lacking CP26 did not depend strongly on the particular pretreatment. In the dataset of particles exposed to the detergent for less than a few minutes [18], a considerable amount of CP26-free supercomplexes were found (Table 1). However, proteolytic activity may also occur in PSII under physiological conditions [30]. It is, of course, possible that the removal of CP26 is caused by the detergent (α-DM), but the time of exposure to this detergent did not influence the occupancy of the CP26 site very much. In our opinion, it should be considered that some of the supercomplexes in the thylakoid membranes may have empty CP26 binding pockets.

The occupancy of the CP24 site was less easy to establish, because CP24 occurs only in the less abundant complexes with trimeric LHCII bound at the M and/or L positions. A class of 54 projections of the C_2S_2M subset (Fig. 3G) lacked a mass of the size of a monomeric LHC protein at the position proposed to be occupied by CP24 [16], whereas a class of nine projections of the C_2S_2L subset (Fig. 3I) missed a mass at about the same position. These data suggest that the CP24 binding pocket can be empty (although the relative occupancy of CP24 seems considerably larger than of CP26; Table 1) and that the structure of the remaining parts of the supercomplexes does not depend on the presence of CP26 or CP24.

We conclude from these observations that CP26 and CP24 are not required for the binding of trimeric LHCII to the dimeric PSII core complex at either the S, M or L position. In contrast, it could even be that the binding of trimeric LHCII at the M or L position is required for the binding of CP24 to the C_2S_2 supercomplex and that the binding of trimeric LHCII at the S position is required for the binding of CP26 to this complex. A search for C_2S_2 supercomplexes with bound CP24 using an artificially prepared projection had a negative result, despite the very large dataset. In addition, C_2S complexes with bound CP26 (or CP29) on the LHCII-free half of the complex have never been found. We note that in supercomplexes obtained from salt- or Tris-washed PSII membranes, the CP26 tip was even more frequently absent than in supercomplexes obtained from oxygen-evolving PSII membranes; a relatively large number of particles could be observed with both sites empty (E. J. Boekema, H. van Roon, J. F. L. van Breemen & J. P. Dekker, unpublished observations).

We have not found 'standard' supercomplexes with an empty CP29 binding pocket in any of the datasets analysed in this work. A search for such complexes in the complete dataset of 16 600 projections using an artificially prepared C_2S_2 supercomplex with an empty CP29 binding position had a negative result.

In conclusion, the results described in this section suggest that trimeric LHCII can only be bound to the dimeric PSII core complex if CP29 is bound, whereas CP26 and CP24 can only be bound if trimeric LHCII is present at the S (CP26) or M or L position (CP24). It thus seems that in the first instance CP29 binds to the dimeric PSII core complex, followed by trimeric LHCII and then CP26 and CP24. This consecutive accumulation of the various LHCII subunits may be important for the understanding of the biogenesis of complete PSII unit (reviewed in [31]).

A third type of megacomplex

In our previous report [19], we described the structural characteristics of two different types of 'megacomplexes'. These complexes were referred to as 'megacomplex type I' and 'megacomplex type II' and were both shown to consist of two C_2S_2M supercomplexes arranged in an antiparallel fashion. The only resolvable difference was a translational shift of about 7.5 nm of one of the C_2S_2M units.

Reclassification of the subset of megacomplexes revealed a completely new type of projection with a 'windmill'-like shape (Fig. 6A). The complexes occurred in small quantities, but could be assigned because of the large number of projections in the present dataset. The new complexes are designated 'megacomplex type III' and they consist of two C_2S_2 supercomplexes connected via their CP26 tips. Figure 6B shows that both CP26 units are probably present at the interface, and that an area of about 2 × 1.5 nm at the tips of the individual C_2S_2 supercomplexes is not present in the megacomplexes. It is very likely that the extra mass in the supercomplexes is caused by detergent molecules at the edges of the individual C_2S_2 supercomplexes [32]; an association of two C_2S_2 supercomplexes lacking CP26 at their interfaces would leave much space unaccounted for (Fig. 6C).

The occurrence of this new type of megacomplex again indicates the heterogeneous nature of the PSII–LHCII association. As in the cases of the other two types of megacomplexes, this association is impossible if trimeric LHCII is bound at the L-position.

Structural variation in the PSII core parts

The very large data set of C_2S_2 supercomplexes obtained from the PSII membranes allowed a more detailed analysis of the PSII core part in the top-view projections. In this region, five densities are visible (Fig. 7D), which we denoted A–E as previously [17]. The densities A and E were attributed to the large extrinsic loops of the CP47 and CP43 subunits, respectively, whereas density B was assigned to the extrinsic 33-kDa oxygen-evolving complex (OEC) protein, and densities C and D to the D1/D2 reaction centre complex [17]. The most recent structural data on the dimeric PSII core complex [33] have essentially confirmed these preliminary assignments. The 23-kDa OEC protein of green plants is thought to be present at density D [17], whereas the extrinsic cytochrome *c*-550 protein of cyanobacteria is probably located at density C [34].

A classification of the core parts of 4273 well-preserved projections of complete C_2S_2 supercomplexes shows that the areas of density C have by far the strongest variation. In almost 25% of the projections, one of the C densities is reduced (Fig. 7B), whereas in fewer than 10% of the particles both densities C are reduced (Fig. 7A). In more than 50% of the particles, substantial density is observed at both positions C (Fig. 7C). Thus, in most projections there is much density at position C, which explains why the view in Fig. 7C does not differ very significantly from the sum of all projections (Fig. 7D). It is unlikely that the variation at density C is caused by staining artefacts, which could be significant for density C in view of its location near the boundary of the complex. Density E, however, is also located near the periphery of the complex and shows no significant structural variation at all. In addition, the variation at density C is not accompanied by variations in the peripheral antenna (Fig. 7A–C). The centre of the variation seems to be located just below (above) the centre of the density at position C at the left (right) side of the complex (Fig. 7E,F).

Structural work using cryoelectron crystallography on a CP47–reaction centre complex [6] and a dimeric oxygen-evolving core complex [33] has revealed that five of the seven 'remaining' transmembrane α-helices of the PSII core complex are located at or near density C. These α-helices do not belong to one of the four large PSII core membrane proteins (D1, D2, CP47, CP43), but to small proteins with a single transmembrane α-helix (most likely the two subunits of cytochrome *b*-559 and the *PsbI*, *PsbK*, *PsbL*, *PsbTc* and *PsbW* proteins [35]). The five proteins involved are probably connected to the D2 and CP47 complexes [33].

As the observed differences are almost totally within the boundaries of the supercomplexes, they can most easily be explained by a partial absence of a hydrophilic subunit. Possible candidates are the 17-kDa OEC protein (which would in this case be located at a similar position as the extrinsic cytochrome *c*-550 protein of cyanobacterial PSII [34]), and possibly a second copy of the 33-kDa OEC protein. The stoichiometry of the latter protein has been a matter of debate [36]. A number of recent biochemical studies have indicated that the stoichiometry must be two per PSII monomer in oxygen-evolving PSII preparations and that the second copy could be located near the inactive side of the complex [37,38], which may be at density C. The location of an additional extrinsic protein at density C does not contradict the side-view images of the PSII–LHCII supercomplexes [17]. The partial absence of an extrinsic protein at density C may be caused by the detergent, which may affect the conformation of the complex near its periphery.

It can, however, not be excluded that another type of variation causes the observed differences at density C, and the partial presence of one or two small proteins with a single transmembrane α-helix could also be responsible for the observed differences. A possible candidate is cytochrome *b*-559, which according to at least some estimates is present in larger complexes than isolated PSII reaction centre complexes at an about 1.5 stoichiometry with the PSII reaction centre (e.g [39]), in which case the second *b*-559 could be responsible for the observed variation.

CONCLUDING REMARKS

Table 1 summarizes our results on the relative occurrence of the various α-DM solubilized PSII–LHCII supercomplexes and megacomplexes. The numbers shown in this table should be regarded as a rather crude estimate of the α-DM solubilization, because some preference in the selection of the particles can not be excluded. In addition, in the third and fourth datasets some of the C_2S_2 supercomplexes lacking CP26 tips were not selected, whereas the second dataset was largely devoid of megacomplexes because of the nature of the pretreatment of the solubilized material. Some features, however, are beyond reasonable doubt, such as the occurrence of the various types of trimeric LHCII (S > M > L), the occurrence of empty binding pockets of monomeric LHCII proteins (CP26 > CP24 > CP29) and the occurrence of the three types of megacomplexes (I > II > III).

This contribution completes the description of the variation in the antenna parts of the PSII–LHCII supercomplexes and megacomplexes at a resolution of slightly better than 2 nm. The variation has been described by multivariate statistical analysis plus classification of negatively stained single particle electron microscopy projections. In the light of the large number of

analysed projections (16 600), further progress may in the first place be expected from a new technique, e.g. cryo-electron microscopy of frozen-hydrated specimens, either stained, or unstained. In principle, these techniques enable extraction of detail at high resolution, and may form a next step on the route leading to the complete assignment of the 25 or more subunits of the complete PSII unit. A prerequisite for an analysis with these types of techniques, however, is a well-defined and homogeneous particle. The work described in this paper indicate that with α-DM, certainly one of the mildest detergents used thus far for solubilization of PSII membranes, the criterion of homogeneity is hard to reach, in view of the various ways by which the peripheral antenna and the PSII core dimer are connected (Table 1). There are significant numbers of particles with either additional trimeric LHCII complexes (in the M and/or L binding positions), or with empty CP26 binding sites. In addition, there is significant variation near the periphery of the PSII core parts of the complexes (the density C in Fig. 7), which could be due to the partial absence of an extrinsic protein or a small transmembrane protein. With β-DM, the heterogeneity in the binding of trimeric LHCII seems less pronounced [18], but on the other hand there is no reason to assume that the heterogeneity at the CP26 binding position and at density C in the PSII core part does not occur with this detergent. In fact, heterogeneity at the CP26 binding position has also been observed with β-DM [40].

With α-DM, however, we have been able to obtain several new details of the organization of the peripheral antenna proteins in the PSII grana membranes, an important step towards an understanding of the flow of the excitation energy from the peripheral antenna to the PSII reaction centre in the thylakoid membranes. It is important to know, however, to what extent the type of PSII membranes [23] used in this work represent the *in vivo* situation. For this reason, we are currently investigating the possibility of performing experiments as described in this paper on α-DM solubilized thylakoid membranes. Although the 'heterogeneity' of projections will certainly increase due to the presence of photosystem I, cytochrome b_6f, ATP synthase and perhaps even other complexes of thylakoid membrane proteins, the possibility of detergent-induced artefacts will be further reduced.

ACKNOWLEDGEMENTS

We thank Prof. A. Brisson for stimulating discussions and Mr K. Gilissen for photography.

REFERENCES

1. Hankamer, B., Barber, J. & Boekema, E.J. (1997) Structure and membrane organization of photosystem II from green plants. *Ann. Rev. Plant Phys. Plant Mol. Biol.* **48**, 641–672.
2. Santini, C., Tidu, V., Tognon, G., Ghiretti Magaldi, A. & Bassi, R. (1994) Three-dimensional organization of the higher plant photosystem II reaction centre and evidence for its dimeric organization *in vivo*. *Eur. J. Biochem.* **221**, 307–315.
3. Peter, G.F. & Thornber, J.P. (1991) Biochemical evidence that the higher plant photosystem II core complex is organized as a dimer. *Plant Cell Physiol.* **32**, 1237–1250.
4. Barber, J. (1998) Photosystem two. *Biochim. Biophys. Acta* **1365**, 269–277.
5. Rhee, K.-H., Morris, E.P., Zheleva, D., Hankamer, B., Kühlbrandt, W. & Barber, J. (1997) Two-dimensional structure of plant photosystem II at 8 Å resolution. *Nature* **389**, 522–526.
6. Rhee, K.-H., Morris, E.P., Barber, J. & Kühlbrandt, W. (1998) Three-dimensional structure of the plant photosystem II reaction centre at 8 Å resolution. *Nature* **396**, 283–286.
7. Barber, J., Nield, J., Morris, E.P. & Hankamer, B. (1999) Subunit positioning in photosystem II revisited. *Trends Biochem. Sci.* **24**, 43–45.
8. Bassi, R., Sandonà, D. & Croce, R. (1997) Novel aspects of chlorophyll *a/b* proteins. *Physiol. Plant.* **100**, 769–779.
9. Jansson, S. (1994) The light-harvesting chlorophyll *a/b* proteins. *Biochim. Biophys. Acta* **1184**, 1–19.
10. Kühlbrandt, W., Wang, D.N. & Fujiyoshi, Y. (1994) Atomic model of plant light-harvesting complex by electron crystallography. *Nature* **367**, 614–621.
11. Kühlbrandt, W. (1994) Structure and function of the plant light-harvesting complex, LHC-II. *Curr. Opin. Struct. Biol.* **4**, 519–528.
12. Sandonà, D., Croce, R., Pagano, A., Crimi, M. & Bassi, R. (1998) Higher plant light-harvesting proteins. Structure and function as revealed by mutation analysis of either protein or chromophore moieties. *Biochim. Biophys. Acta* **1365**, 207–214.
13. Boekema, E.J., Hankamer, B., Bald, D., Kruip, J., Nield, J., Boonstra, A.F., Barber, J. & Rögner, M. (1995) Supramolecular structure of the photosystem II complex from green plants and cyanobacteria. *Proc. Natl Acad. Sci. USA* **92**, 175–179.
14. Hankamer, B., Nield, J., Zheleva, D., Boekema, E.J., Jansson, S. & Barber, J. (1997) Isolation and characterization of monomeric and dimeric photosystem II complexes from spinach and their relevance to the organisation of Photosystem II *in vivo*. *Eur. J. Biochem.* **243**, 422–429.
15. Eshaghi, S., Andersson, B. & Barber, J. (1999) Isolation of a highly active PSII-LHCII supercomplex from thylakoid membranes by a direct method. *FEBS Lett.* **446**, 23–26.
16. Harrer, R., Bassi, R., Testi, M.G. & Schäfer, C. (1998) Nearest-neighbour analysis of a photosystem II complex from *Marchantia polymorpha* L. (liverwort), which contains reaction centre and antenna proteins. *Eur. J. Biochem.* **255**, 196–205.
17. Boekema, E.J., Nield, J., Hankamer, B. & Barber, J. (1998) Localization of the 23 kDa subunit of the oxygen evolving complex of photosystem II by electron microscopy. *Eur. J. Biochem.* **252**, 268–276.
18. Boekema, E.J. & van Roon, H. & Dekker, J.P. (1998) Specific association of photosystem II and light-harvesting complex II in partially solubilized photosystem II membranes. *FEBS Lett.* **424**, 95–99.
19. Boekema, E.J. & van Roon, H., Calkoen, F., Bassi, R. & Dekker, J.P. (1999) Multiple types of association of photosystem II and its light-harvesting antenna in partially solubilized photosystem II membranes. *Biochemistry* **38**, 2233–2239.
20. Dekker, J.P., van Roon, H. & Boekema, E.J. (1999) Heptameric association of light-harvesting complex II trimers in partially solubilized photosystem II membranes. *FEBS Lett.* **449**, 211–214.
21. Dekker, J.P., van Roon, H. & Boekema, E.J. (1998) Structural characterization of megacomplexes of photosystem II and LHCII of grana membranes from spinach. In *Photosynthesis: Mechanisms and Effects* (Garab, G., ed.), pp. 301–304. Kluwer Academic Publishers, Dordrecht, the Netherlands.
22. Boekema, E.J. & van Roon, H. & Dekker, J.P. (1998) Refined analysis of supercomplexes of photosystem II and LHCII of grana membranes from spinach. In *Photosynthesis: Mechanisms and Effects* (Garab, G., ed.), pp. 305–308. Kluwer Academic Publishers, Dordrecht, the Netherlands.
23. Berthold, D.A., Babcock, G.T. & Yocum, C.F. (1981) A highly resolved, oxygen-evolving photosystem II preparation from spinach thylakoid membranes. EPR and electron transport properties. *FEBS Lett.* **134**, 231–234.
24. Eijckelhoff, C., van Roon, H., Groot, M.-L. & van Grondelle, R. & Dekker, J.P. (1996) Purification and spectroscopic characterization of photosystem II reaction centre complexes isolated with or without Triton X-100. *Biochemistry* **35**, 12864–12872.
25. Harauz, G., Boekema, E. & van Heel, M. (1988) Statistical image

analysis of electron micrographs of ribosomal subunits. *Methods Enzymol.* **164**, 35–49.

26. Van Heel, M. (1987) Similarity between images. *Ultramicroscopy* **21**, 95–100.
27. Kühlbrandt, W. (1988) Structure of light-harvesting chlorophyll *a/b* protein complex from plant photosynthetic membranes at 7 Å resolution in projection. *J. Mol. Biol.* **202**, 849–864.
28. Peter, G.F. & Thornber, J.P. (1991) Biochemical composition and organization of higher plant photosystem II light-harvesting pigment proteins. *J. Biol. Chem.* **266**, 16745–16754.
29. Bassi, R. & Dainese, P. (1992) A supramolecular light-harvesting complex from chloroplast photosystem II membranes. *Eur. J. Biochem.* **204**, 317–326.
30. Andersson, B. & Aro, E.-M. (1997) Proteolytic activities and proteases of plant chloroplasts. *Physiol. Plant.* **100**, 780–793.
31. Wollman, F.-A., Minai, L. & Nechustai, R. (1999) The biogenesis and assembly of photosynthetic proteins in thylakoid membranes. *Biochim. Biophys. Acta* **1411**, 21–85.
32. Dekker, J.P., Boekema, E.J., Witt, H.T. & Rögner, M. (1988) Refined purification and further characterization of oxygen-evolving and Tris-treated photosystem II particles from the thermophilic cyanobacterium *Synechococcus* sp. *Biochim. Biophys. Acta* **936**, 307–318.
33. Hankamer, B., Morris, E.P. & Barber, J. (1999) Revealing the structure of the oxygen-evolving core dimer of photosystem II by cryoelectron crystallography. *Nat. Struct. Biol.* **6**, 560–564.
34. Kuhl, H., Rögner, M., van Breemen, J.F.L. & Boekema, E.J. (1999) Localization of cyanobacterial photosystem II donor-side subunits by electron microscopy and the supramolecular organization of photosystem II in the thylakoid membrane. *Eur. J. Biochem.*, **266**, 453–459.
35. Zheleva, D., Sharma, J., Panico, M., Morris, H.R. & Barber, J. (1998) Isolation and characterization of monomeric and dimeric CP47-reaction centre photosystem II complexes. *J. Biol. Chem.* **273**, 16122–16127.
36. Seidler, A. (1996) The extrinsic polypeptides of photosystem II. *Biochim. Biophys. Acta* **1277**, 35–60.
37. Betts, S.D., Ross, J.R., Pichersky, E. & Yocum, C.F. (1997) Mutation Val235Ala weakens binding of the 33-kDa manganese stabilizing protein of photosystem II to one of two sites. *Biochemistry* **36**, 4047–4053.
38. Bricker, T.M. & Frankel, L.K. (1998) The structure and function of the 33 kDa extrinsic protein of photosystem II: a critical assessment. *Photosynth. Res.* **56**, 157–173.
39. Van Leeuwen, P.J., Nieveen, M.C. & van de Meent, E.J. Dekker, J.P. & van Gorkom, H.J. (1991) Rapid and simple isolation of pure photosystem II core and reaction center particles from spinach. *Photosynth. Res.* **28**, 149–153.
40. Boekema, E.J., Hankamer, B., Nield, J. & Barber, J. (1995) Photosystem II structure investigated by electron microscopy and single-particle averaging. In *Photosynthesis: from Light to Biosphere* (Mathis, P., ed.), Vol. III, pp. 229–232. Kluwer Academic Publishers, Dordrecht, the Netherlands.